EUROFUSION WPJET1-CP(16) 14937

H Urano et al.

Global stabilization effect of Shafranov shift on the edge pedestal plasmas in JET and JT-60U

Preprint of Paper to be submitted for publication in Proceedings of 26th IAEA Fusion Energy Conference

This work has been carried out within the framework of the EUROfusion Consortium and has received funding from the Euratom research and training programme 2014-2018 under grant agreement No 633053. The views and opinions expressed herein do not necessarily reflect those of the European Commission.

Global stabilization effect of Shafranov shift on the edge pedestal plasmas in JET and JT-60U

H. Urano[1], S. Saarelma[2], L. Frassinetti[3], N. Aiba[4], C.F. Maggi[2], I.T. Chapman[2], I. Lupelli[2], C. Challis[2], M. Leyland[5], M. Beurskens[6], K. Kamiya[1], C. Giroud[2], S. Pamela[2], JT-60 Team[1] and JET Contributors[†]

EUROfusion Consortium, JET, Culham Science Centre, Abingdon, OX14 3DB, UK

[1] National Institutes for Quantum Radiological Science and Technology, Naka, 311-0193, Japan

[2] Culham Centre for Fusion Energy, Culham Science Centre, Abingdon OX14 3DB, UK

[3] Division of Fusion Plasma Physics, KTH Royal Institute of Technology, Stockholm, Sweden

[4] National Institutes for Quantum Radiological Science and Technology, Rokkasho, 039-3212, Japan

[5] York Plasma Institute, University of York, Heslington, York, YO10 5DD, UK

[6] Max-Planck-Institut fur Plasmaphysik, Wendelsteinstr. 1, D-17491, Greifswald, Germany

[†] See the author list of "Overview of the JET results in support to ITER" by X. Litaudon et al. to be published in Nuclear Fusion Special issue: overview and summary reports from the 26th Fusion Energy Conference (Kyoto, Japan, 17-22 October 2016)

e-mail contact of main author: `urano.hajime@qst.go.jp`

The effect of Shafranov shift on the pedestal structure was examined in the variation of the plasma shape in JET and JT-60U. The stabilization of $\beta_{\rm p}$ or Shafranov shift becomes effective in hybrid operation at relatively low I_p. Independently of κ, the pedestal pressure $p_{\rm ped}$ is raised by high δ at high $\beta_{\rm p}$. At high κ, the difference of the edge pressure gradient between low and high δ is clearer at high $\beta_{\rm p}$ whereas the pedestal width is nearly unchanged. On the other hand, the stability limit of the edge pressure gradient is reduced by low κ at high n ballooning mode whereas the pedestal expands. A wider pedestal is formed at lower δ at fixed $\beta_{\rm p,ped}$. At high δ and low κ, the pedestal expands more largely than the conventional scaling. The pedestal expansion is observed when the pedestal is destabilized by high n ballooning mode. Low κ brings the pedestal unstable against high n ballooning mode and close to grassy ELM regime at high δ, high q_{95} and high $\beta_{\rm p}$.

1. Introduction

In the present understanding, H-mode confinement is determined by the edge and core interplay [1, 2]. The pedestal structure is determined by the edge stability and plays a role as a boundary condition in determining the core confinement through profile stiffness. On the other hand, the increased $\beta_{\rm p}$ or Shafranov shift stabilizes the pedestal plasma.

The effect of Shafranov shift on the pedestal has been examined by the stability analysis in which the core pressure is artificially increased whereas the pedestal profile is kept fixed [3, 4]. However, it is still unknown how effectively the Shafranov shift works on the pedestal depending on the plasma shape. In this paper, we examine the effect of the Shafranov shift on the pedestal in the variation of the plasma shape using JET and JT-60U tokamaks.

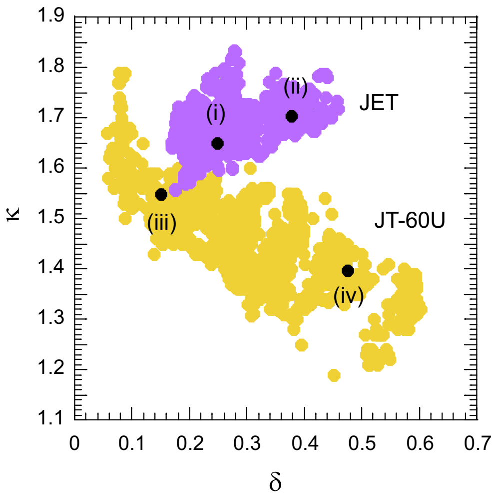

FIG. 1: Operational space of the triangularity δ and ellipticity κ in JET and JT-60U.

As shown in figure 1, there is a large difference in the operational space of the triangularity δ and ellipticity κ between JET and JT-60U in spite of the similar machine size. In JET, δ is varied from 0.15 to 0.45 at relatively high κ of $1.6-1.8$. On the other hand, JT-60U has a wide variation of $\delta(=0.05-0.6)$ at relatively low κ whereas there is an anti-collinearity between δ and κ, which arises from the technical constraint of the poloidal coil system.

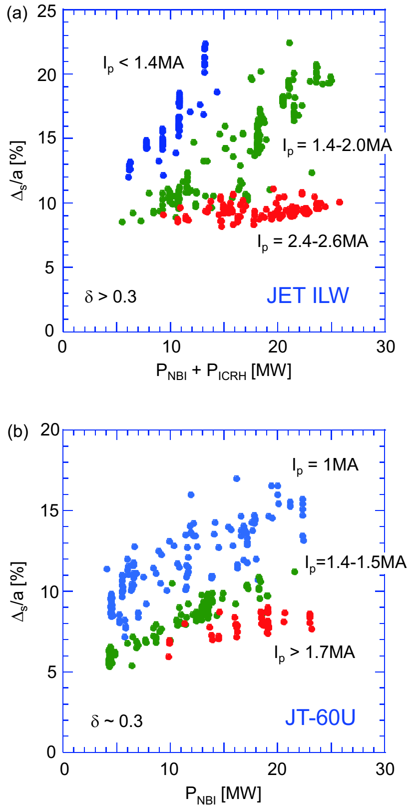

FIG. 2: Shafranov shift as a function of the heating power in the variation of I_p in (a) JET and (b) JT-60U.

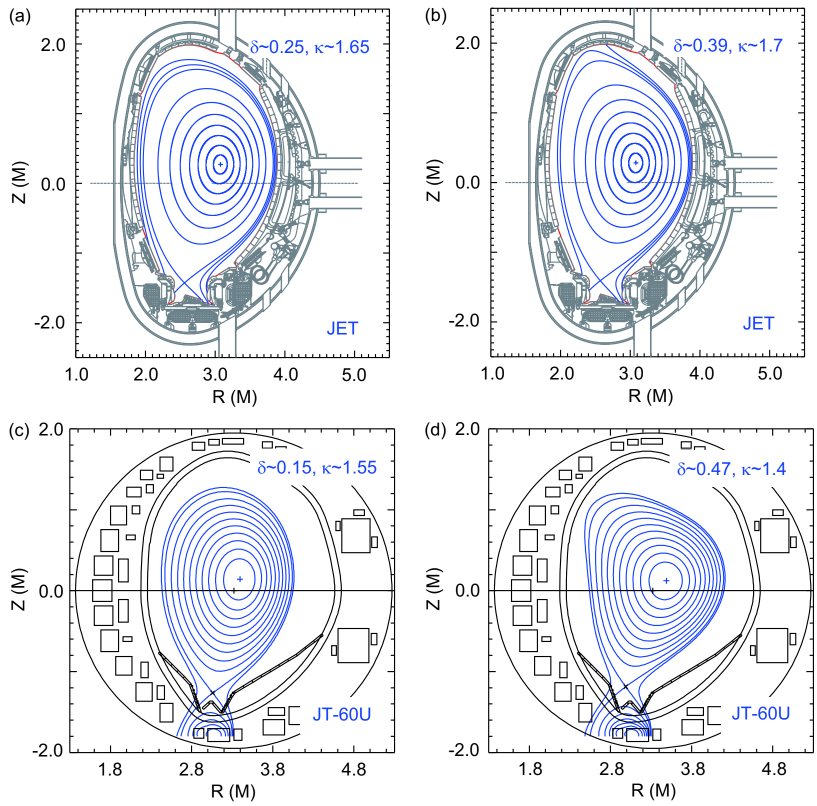

FIG. 3: Four plasma shapes employed to examine the effect of the Shafranov shift on the pedestal. The data points of (i)-(iv) in figure 1 correspond to (a)-(d) in this figure, respectively.

Besides, the edge pedestal plasmas in the main operational regime of both devices become generally unstable against the ballooning component of the peeling-ballooning mode (PBM), which is mainly stabilized by the increased β_p or Shafranov shift. Therefore, these two devices are chosen to examine the effect of the Shafranov shift on the pedestal in the variation of the plasma shape. Note that all the JET data in this study were taken from the ITER-like-wall experiments.

2. Experiments

Figure 2 shows the normalized Shafranov shift Δ_s/a as a function of the heating power in the variation of the plasma current I_p in both devices. The change of Shafranov shift depends clearly on I_p. The Shafranov shift can more easily be increased by high power at lower I_p, whereas it is increased only very weakly at higher I_p. Hence, the stabilization of the Shafranov shift requires the operation at relatively low I_p and high β_p. The effect of the Shafranov shift more easily appears in the hybrid operation than the baseline scenario. In order to keep a wide range of β_p or Δ_s/a, we focus on the experiments at relatively low I_p with a wide variation of the heating power. In addition, four plasma shapes were selected for this study as shown in figure 3, i.e. (a) low $\delta(\sim 0.25)$ and high $\kappa(\sim 1.65)$, (b) high $\delta(\sim 0.39)$ and high $\kappa(\sim 1.7)$, (c) low $\delta(\sim 0.15)$ and medium $\kappa(\sim 1.55)$ and (d) high $\delta(\sim 0.47)$ and low $\kappa(\sim 1.4)$. The target experimental condition in JET was selected at $I_\mathrm{p} = 1.4$MA, $B_\mathrm{t} = 1.7$T, $q_{95} \sim 3.9$ and $P_\mathrm{NBI} = 5 - 16$MW [5]. Similarly, the condition in JT-60U was selected at $I_\mathrm{p} = 1.0$MA, $B_\mathrm{t} = 2.1$T, $q_{95} \sim 3.7$ and $P_\mathrm{NBI} = 6 - 15$MW.

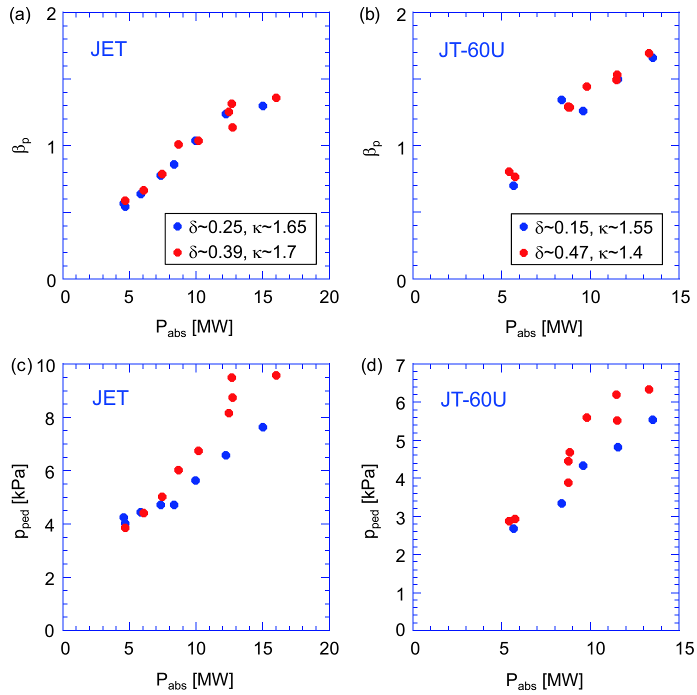

FIG. 4: Dependence of global β_p and p_{pped} on P_{abs} in the variation of the plasma shape.

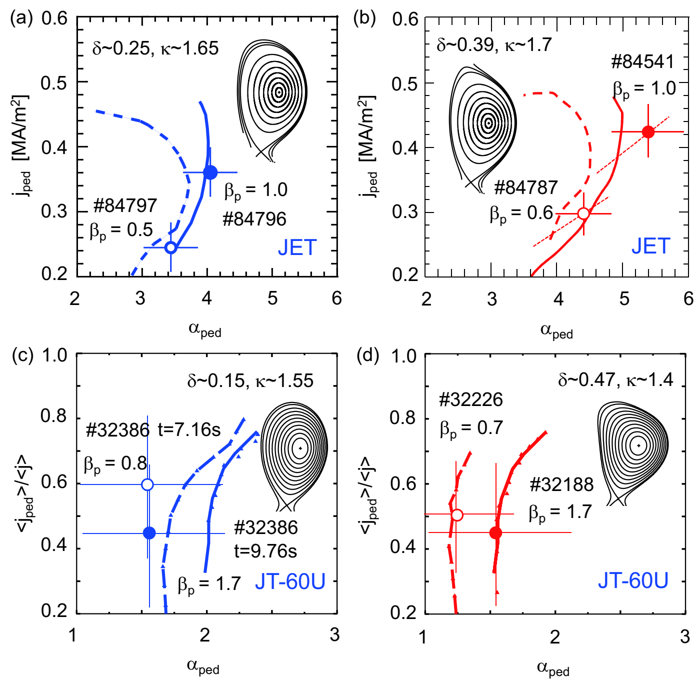

FIG. 5: Edge MHD stability diagrams in $j - \alpha$ space at low and high β_p for four plasma shapes cases.

3. Edge pedestal characteristics with increased β_p

Figures 4(a) and (b) show the dependence of β_p on the plasma absorbed power P_{abs} in JET and JT-60U. The global β_p increases with the heating power for all the plasma shapes of low and high δ. There is no large difference in β_p between low and high δ at fixed P_{abs}. Figures 4(c) and (d) show the dependence of the pedestal pressure p_{ped} on P_{abs} in JET and JT-60U. Independently of κ, the pedestal pressure is raised at high δ with increased heating power. Note that the difference in the pedestal pressure is negligible between low and high δ at low P_{abs} whereas high δ shape becomes more effective with increased P_{abs} [6, 7]. In other

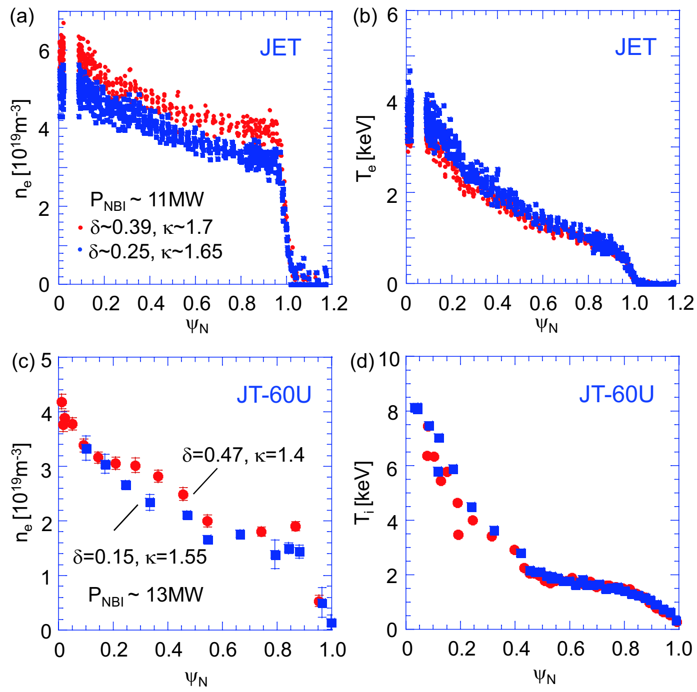

FIG. 6: Spatial profiles of the electron density $\bar{n}_e$ and the electron temperature T_e, or the ion temperature T_i for low and high δ at high β_p.

words, higher pedestal pressure can be obtained by high δ configuration at a given β_p for both devices.

Next, we compare the dependence of the edge MHD stability boundaries on β_p among the different plasma shapes. Figures 5(a) and (b) show the edge MHD stability diagram of the peeling-ballooning mode in $j - \alpha$ space calculated by ELITE for low and high δ cases in JET, respectively. Similarly, figures 5(c) and (d) show the edge $j - \alpha$ diagram calculated by MARG2D for low and high δ cases in JT-60U, respectively. The global β_p changes roughly twice. The stability limit of the normalized edge pressure gradient is raised by the stabilization effect of the increased Shafranov shift for all types of plasma shape, independently of κ. Particularly at high κ in JET, the experimentally measured edge pressure gradient is raised more strongly by increased β_p at higher δ. One may notice that the stable region at fixed β_p of 1.0 expands with increased δ at high κ (see figures 5(a) and (b)) whereas the stable region at fixed β_p of 1.7 shrunk with increased δ and reduced κ (see figures 5(c) and (d)). The difference in the edge stability boundary among the plasma shapes at high β_p is discussed later.

4. Dependence of pedestal characteristics on plasma shape at high β_p

As shown in figure 4, higher δ H-mode plasmas have relatively higher pedestal pressure at high heating power. Figure 6 shows the spatial profiles of the electron density $\bar{n}_e$ and the electron temperature T_e, or the ion temperature T_i for low and high δ at high heating power. In this figure, these spatial profiles are compared between low and high δ plasmas for each device whereas the other experimental conditions are nearly fixed. As expected from figures 4(a) and (b), the global β_p values are also the same at ~ 1.0 in JET and ~ 1.4 in JT-60U. We can find that, independently of κ, high δ configuration leads to higher density from the edge pedestal to the core plasma [11]. On the other hand, the T_e or T_i profile does not change significantly or the core temperature becomes lower slightly at high δ. Thus, the increased pedestal pressure at high δ and high β_p shown in figures 4(c) and (d) is mainly

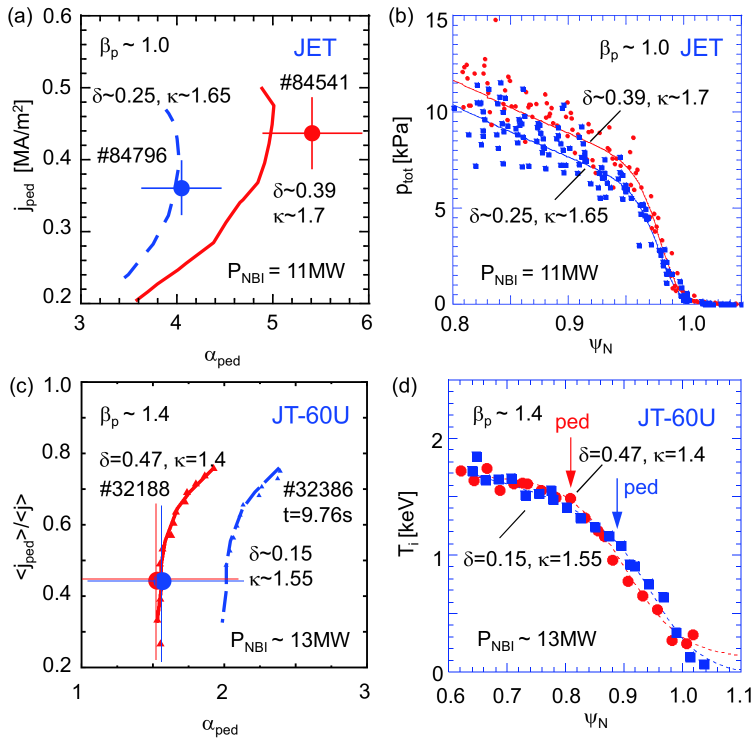

FIG. 7: Edge MHD stability diagrams in $j-\alpha$ space at low and high δ at high β_p.

attributed to the increased density.

Next, we compare the dependence of the edge MHD stability boundaries on the plasma shape at fixed β_p. Figures 7(a) and (b) show the edge $j-\alpha$ diagram of the peeling-ballooning mode and the edge pressure profiles for low and high δ cases at the global β_p of ~ 1.0 in JET, respectively. Even at fixed β_p, larger edge pressure gradient is obtained at higher δ due to the expansion of the stable region. However, one can find that pedestal width is nearly the same between low and high δ (see figure 7(b)). Thus, the increase of the pedestal pressure at high δ and high β_p in JET shown in figure 4(c) is attributed to the increased edge pressure gradient due to the global β_p stabilization with nearly no change in the pedestal width.

On the other hand, figures 7(c) and (d) show the edge $j-\alpha$ diagram and the edge T_i profiles for low δ (medium κ) and high δ (low κ) cases at the global β_p of ~ 1.4 in JT-60U, respectively. At fixed β_p, the edge MHD stability limit of the edge pressure gradient is reduced by low κ even for high δ case. Reduced κ makes the ideal ballooning mode and/or the ballooning component of the peeling-ballooning mode at high toroidal mode number more strongly unstable than the stabilization due to high δ [9]. However, as shown in figure 7(d), the high δ case shows a wider pedestal in the T_i profile at lower gradient, so that the pedestal pressure is kept high (see figure 4(d)).

5. Expansion of pedestal width at high β_p

Figures 8(a) and (c) show the dependence of the pedestal width in the normalized poloidal flux space $\Delta_{\psi\mathrm{N}}$ on P_abs for low and high δ cases in JET and JT-60U, respectively. In JET, although the pedestal width expands with increased heating power for both shapes, there is no large difference in the pedestal width between low and high δ at fixed P_abs or global β_p. On the other hand, the pedestal width at high δ and low κ expands more strongly with increased P_abs than that at low δ and medium κ in JT-60U. Thus, there is no large difference in the pedestal width between low and high δ at low P_abs whereas a wide pedestal is formed

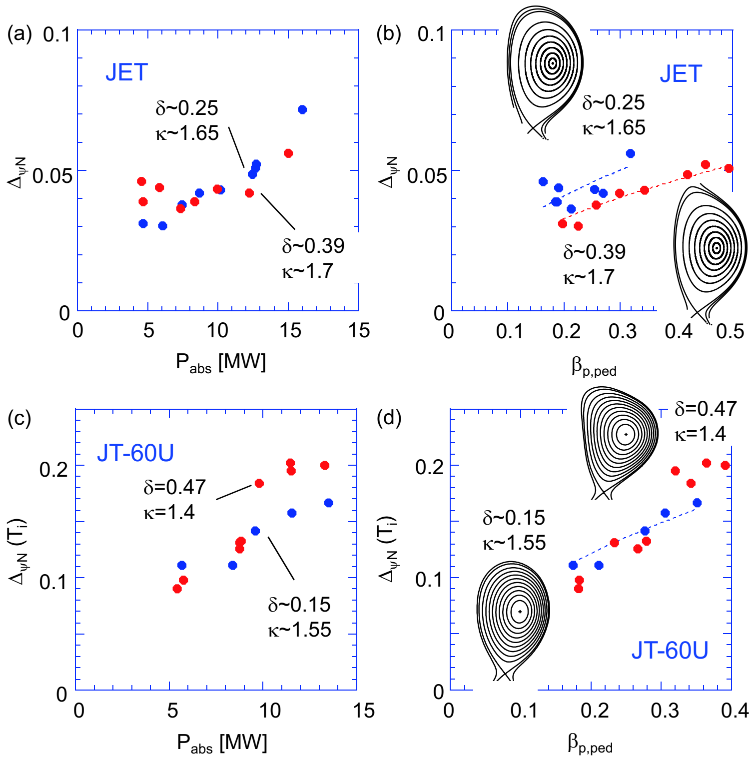

FIG. 8: Pedestal width as a function of (a) $P_{\rm abs}$ and (b) $\beta_{\rm p,ped}$ for low and high δ in JET. Pedestal width as a function of (a) $P_{\rm abs}$ and (b) $\beta_{\rm p,ped}$ for low δ (medium κ) and high δ (low κ) in JT-60U.

in the high δ and low κ case at high $P_{\rm abs}$ or high $\beta_{\rm p}$.

Figures 8(b) and (d) show the relationship between $\Delta_{\psi{\rm N}}$ and the pedestal poloidal beta $\beta_{\rm p,ped}$ in JET and JT-60U, respectively. It has prevalently been recognized that the pedestal width varies in proportion to $\beta_{\rm p,ped}^{1/2}$ [2, 10]. In JET, the pedestal expands along the scaling of $\Delta_{\psi{\rm N}} \propto \beta_{\rm p,ped}^{1/2}$. However, the result indicates that the proportional coefficient depends on the plasma shape. Relatively a wider pedestal is formed for the low δ case than that for the high δ case at given $\beta_{\rm p,ped}$. This result is consistent with the steeper edge pressure gradient and high pedestal pressure at high δ with nearly the same pedestal width as low δ shown in figure 7(b). In JT-60U, the pedestal width is increased along the scaling of $\Delta_{\psi{\rm N}} \propto \beta_{\rm p,ped}^{1/2}$ for the low δ and medium κ case. However, at high δ and low κ, the pedestal expands more largely than the conventional scaling.

6. Discussion

The unique characteristic of the pedestal widening with reduced edge pressure gradient at high δ and low κ in JT-60U is accompanied by the destabilization of high n ballooning mode due to the reduction of κ as shown in figure 7(c). A similar kind of pedestal widening has also been observed when the edge collisionality ν^* is raised. Figure 9(a) shows the edge $j - \alpha$ diagram for low $\nu^*(= 0.22)$ and high $\nu^*(= 0.67)$ cases at fixed $\beta_{\rm p,ped}$ of ~ 0.3 in JT-60U [11]. As ν^* is raised at fixed $\beta_{\rm p,ped}$, the edge pressure gradient and current density are reduced along the stability boundary with increasing the most unstable toroidal mode number. Figure 9(b) shows the dependence of the pedestal width $\Delta_{\psi{\rm N}}$ on ν^* at fixed $\beta_{\rm p,ped}$. In the ITER relevant low ν^* regime ($\nu^* < 0.1$) where the pedestal becomes unstable against the intermediate n peeling-ballooning mode, the pedestal width is not significantly affected by ν^*. However, at high $\nu^*(> 0.1)$ where the pedestal becomes unstable against the high

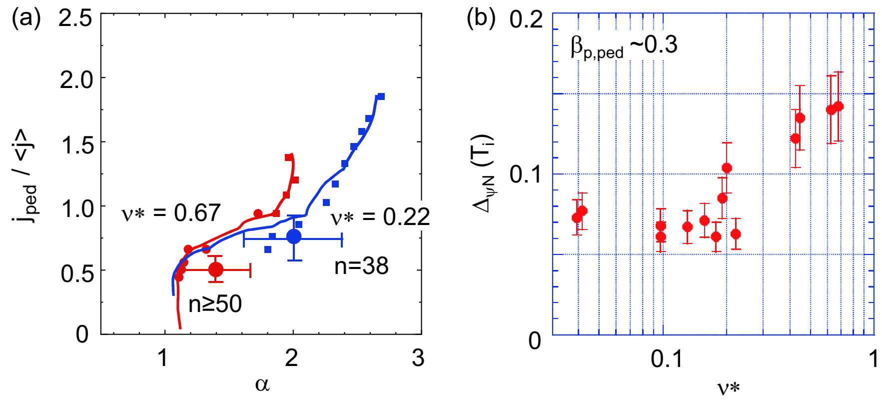

FIG. 9: (a) Edge MHD stability diagrams in $j-\alpha$ space at low and high ν^* at fixed $\beta_{\rm p,ped}$ of 0.3 in JT-60U. (b) Dependence of the pedestal width $\Delta_{\psi\rm N}$ on ν^* at fixed $\beta_{\rm p,ped}$.

n ballooning mode, the pedestal width expands with ν^* even at fixed $\beta_{\rm p,ped}$. The similar experimental result of the pedestal widening is also obtained in gas scan and ν^* scan in JET [12–14]. In the gas scan, the pedestal expands with increased gas puffing rate whereas the pedestal pressure remains constant.

It should be noted that this pedestal expansion occurs in the condition where the pedestal is unstable against high n ballooning mode in both devices. There may be a common physics picture with the pedestal expansion at high $\beta_{\rm p}$ and low κ in JT-60U, where the pedestal is also destabilized by high n ballooning mode due to the reduction of κ (see figure 7(c)).

A schematic view of the pedestal structure at high $\beta_{\rm p}$ in the variation of the plasma shape is illustrated in figure 10. When δ is raised at fixed κ, the pedestal width is nearly the same and the edge pressure gradient is raised due to the stability improvement. In this case, ELM frequency $f_{\rm ELM}$ is reduced as shown in figure 10(a). On the other hand, when δ is raised with reduced κ, the pedestal width is increased and the edge pressure gradient is not raised or reduced because the pedestal is destabilized by high n ballooning mode due to reduced κ. This is consistent with the observation of largely increased $f_{\rm ELM}$ at high δ and low κ (see figure 10(b)). Besides, the condition of high $\delta(>0.4)$ (low κ), high $q_{95}(>4)$ and high $\beta_{\rm p}$ brings the pedestal close to more grassy ELM regime in JT-60U [15]. Considering that grassy ELMs are generated by high n ballooning mode, low κ is a key to bring the pedestal in this regime.

7. Conclusions

The effect of increased Shafranov shift on the pedestal structure was examined in the variation of the plasma shape using JET and JT-60U.

The pedestal stabilization of $\beta_{\rm p}$ or Shafranov shift becomes effective in hybrid operation at relatively low I_p. Independently of κ, the pedestal pressure is raised by high δ at high $\beta_{\rm p}$ whereas the difference was small at low $\beta_{\rm p}$. The increased pedestal pressure at high δ is mainly attributed to the increased density. At high κ in JET, the edge pressure gradient is raised more largely at high δ by the stabilization of the ballooning component of the peeling-ballooning mode due to increased $\beta_{\rm p}$, whereas the pedestal width is nearly unchanged. On the other hand, the stability limit of the edge pressure gradient is reduced at high δ and low κ in JT-60U because the pedestal is destabilized more strongly by high n ballooning mode due to reduced κ, whereas the pedestal expands so that the pedestal pressure is kept high. Except for the low κ case in JT-60U, the pedestal expands along the scaling of $\Delta_{\psi\rm N} \propto \beta_{\rm p,ped}^{1/2}$. However, the pedestal expands with reduced δ at fixed $\beta_{\rm p,ped}$ in JET. At high δ and low κ in

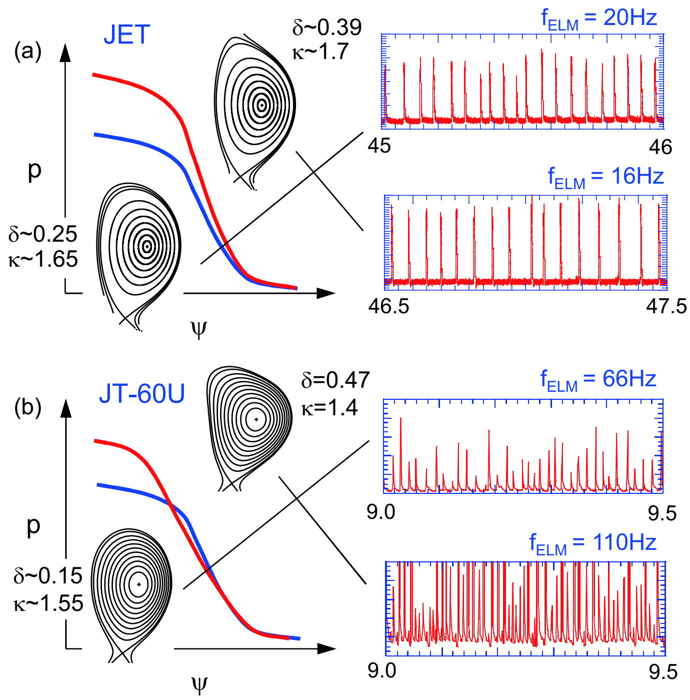

FIG. 10: A schematic view of the pedestal structure at high $\beta_{\rm p}$ in the variation of the plasma shape for (a) JET and (b) JT-60U.

JT-60U, the pedestal expands more largely than the conventional scaling. In gas puff / ν^* scan, the pedestal expansion occurs in the condition where the pedestal is unstable against high n ballooning mode in both devices. There may be a common physics picture with the pedestal expansion at high $\beta_{\rm p}$ and low κ in JT-60U, where the pedestal is also destabilized by high n ballooning mode due to the reduction of κ. The operation at low κ brings the pedestal unstable against high n ballooning mode and close to grassy ELM regime at high δ, high q_{95} and high $\beta_{\rm p}$.

This work has been carried out within the framework of the EUROfusion Consortium and has received funding from the Euratom research and training programme 2014-2018 under grant agreement No 633053. The views and opinions expressed herein do not necessarily reflect those of the European Commission.

References

[1] Maggi, C.F., et al., Nucl. Fusion **47** (2007) 535.
[2] Urano, H., Nucl. Fusion **54** (2014) 116001.
[3] Saarelma, S., et al., Proc. 14th Int. Workshop on H-mode Physics and Transport Barriers (Fukuoka, Japan, 2013) P03-02.
[4] Chapman, I.T., et al., Nucl. Fusion **55** (2015) 013004.
[5] Challis, C., et al., Nucl. Fusion **55** (2015) 053031.
[6] Saibene, G., et al., Nucl. Fusion **39** (1999) 1133.
[7] Urano, H., et al., Plasma Phys. Control. Fusion **44** (2002) 11.
[8] Urano, H., et al., Proc. 42nd Eur. Conf. Plasma Phys. (Leuven, Belgium, 2016) EPS, Geneva O4.121.
[9] Aiba, N., et al., Nucl. Fusion **52** (2012) 114002.
[10] Snyder, P.B., et al., Phys. Plasmas **16** (2009) 056118.
[11] Urano, H., et al., Nucl. Fusion **56** (2016) 016005.
[12] Leyland, M.J., et al., Nucl. Fusion **55** (2015) 013019.
[13] Frassinetti, L., et al., Nucl. Fusion (in press).
[14] Maggi, C.F., et al., this conference.
[15] Oyama, N., et al., Nucl. Fusion **50** (2010) 064014.